Band gaps and refractive indices of AlGaAsSb, GaInAsSb, and InPAsSb: Key properties for a variety of the 2–4-μm optoelectronic device applications

Sadao Adachi
NTT Atsugi Electrical Communications Laboratories, Nippon Telegraph and Telephone Corporation, Atsugi-shi, Kanagawa 243-01, Japan

(Received 10 November 1986; accepted for publication 27 January 1987)

The methods for calculation of material parameters in compound alloys are discussed, and the results for $Al_xGa_{1-x}As_ySb_{1-y}$, $Ga_xIn_{1-x}As_ySb_{1-y}$, and $InP_xAs_ySb_{1-x-y}$ quaternaries lattice matched to GaSb and InAs are presented. These quaternary systems may provide the basis for optoelectronic devices operating over the 2–4-μm wavelength range. The material parameters considered are: the lattice constant, the lowest direct- and indirect-gap energies, and the refractive index. The model used is based on an interpolation scheme, and the effects of compositional variations are properly taken into account in the calculations. Key properties of the material parameters for a variety of optoelectronic device applications are also discussed in detail.

I. INTRODUCTION

Recently a great deal of interest in light sources and detectors in the 2–4-μm wavelength region has been receiving attention, because the development of new fibers, such as fluoride glass fibers, holds the promise of extremely low transmission losses in this wavelength region.[1] The $Al_xGa_{1-x}As_ySb_{1-y}$, $Ga_xIn_{1-x}As_ySb_{1-y}$, and $InP_xAs_ySb_{1-x-y}$ quaternaries lattice matched to GaSb or InAs may provide the basis for devices operating over this entire wavelength range. However, optoelectronic device parameters in such quaternary systems have been hampered by a lack of definite knowledge of many various material parameters.

In our previous papers,[2] we obtained various material parameters of $Al_xGa_{1-x}As$ and $In_{1-x}Ga_xAs_yP_{1-x}$ alloys from an interpolation scheme and found a good agreement with the experimental data. Although the interpolation scheme is still open to experimental verification, it provides more useful and reliable material parameters over the entire range of alloy composition. We also reported calculations for the refractive indices of these alloys at energies below the lowest band gaps.[2,3] The method is based on the calculation of the imaginary part of the dielectric constant ϵ_2, and on using the Kramers–Kronig relations in order to obtain the real part ϵ_1. These methods held promise of being applied to other semiconductor alloys.

The purpose of this paper is to present several material parameters of $Al_xGa_{1-x}As_ySb_{1-y}$, $Ga_xIn_{1-x}As_ySb_{1-y}$, and $InP_xAs_ySb_{1-x-y}$ quaternary alloys lattice matched to GaSb and InAs. The parameters to be presented are: the lattice constant, the band-gap energy, and the refractive index. The band-gap energy is known to be one of the most important device parameters because it is strongly connected with the operating wavelength of the optoelectronic devices.[4] Knowledge of the refractive indices also forms an important part in the design of heterostructure lasers, as well as other waveguiding devices.[4] This paper will present the band-gap energies of not only the lowest direct gap E_0 ($\Gamma-\Gamma$), but also the lowest indirect gaps E_g^X ($\Gamma-X$) and E_g^L ($\Gamma-L$) over the entire range of alloy composition. The contribution to ϵ_2 of the interband transitions, near the band extrema ($E_0/E_0+\Delta_0$, $E_1/E_1+\Delta_1$, and E_2), is taken into account in this model. This enables us to obtain information on the optical constants over the entire spectral region, i.e., below and above the lowest band edge. The resultant analytical expressions are used to calculate the dispersion of the refractive indices for the quaternary alloys.

II. THEORETICAL MODEL

A. Refractive index

The dielectric function, $\epsilon(\omega)=\epsilon_1(\omega)+\epsilon_2(\omega)$, is known to describe the optical response of the medium at all photon energies $E=\hbar\omega$. Real and imaginary parts of this dielectric function are connected by the Kramers–Kronig relations

$$\epsilon_1(\omega)-1=\frac{2}{\pi}\int_0^\infty \frac{\omega'\epsilon_2(\omega')}{(\omega')^2-\omega^2}\,d\omega', \tag{1a}$$

$$\epsilon_2(\omega)=-\frac{2}{\pi}\int_0^\infty \frac{\epsilon_1(\omega')}{(\omega')^2-\omega^2}\,d\omega'. \tag{1b}$$

The dielectric function is strongly connected with the electronic energy-band structures of the material. The optical joint density of states becomes large for electronic transitions in the neighborhood of critical points (CP's). The lowest direct gaps E_0 and $E_0+\Delta_0$ are of the three-dimensional (3D) M_0 type CP's. Assuming the bands are parabolic, we obtain the contribution of these gaps to $\epsilon_1(\omega)$ and $\epsilon_2(\omega)$ (Ref. 3):

$$\epsilon_1(\omega)-1=AE_0^{-1.5}\times[f(\chi_0)+\tfrac{1}{2}[E_0/(E_0+\Delta_0)]^{1.5}f(\chi_{os})], \tag{2}$$

$$\epsilon_2=[A/(\hbar\omega)^2]\,[(\hbar\omega-E_0)^{0.5}H(\chi_0-1)+\tfrac{1}{2}(\hbar\omega-E_0-\Delta_0)^{0.5}H(\chi_{os}-1)], \tag{3}$$

with

$$A=\tfrac{4}{3}(\tfrac{3}{2}m^*)^{1.5}P^2, \tag{4}$$

 0021-8979/87/104869-08$02.40

$$f(\chi_0) = \chi_0^{-2}\,[2 - (1+\chi_0)^{0.5} - (1-\chi_0)^{0.5} H(1-\chi_0)], \tag{5a}$$

$$f(\chi_{os}) = \chi_{os}^{-2}[2 - (1+\chi_{os})^{0.5} - (1-\chi_{os})^{0.5} H(1-\chi_{os})], \tag{5b}$$

$$\chi_0 = \hbar\omega/E_0, \tag{6a}$$

$$\chi_{os} = \hbar\omega/(E_0 + \Delta_0), \tag{6b}$$

and

$$H(y) = \begin{cases} 1 & \text{for } y \geqslant 0 \\ 0 & \text{for } y < 0. \end{cases} \tag{7}$$

In Eq. (4), m^* is the combined density-of-states mass and P^2 is the squared momentum matrix element.

Band-structure calculations and some experimental work indicated that the E_1 and $E_1 + \Delta_1$ transitions take place along the ⟨111⟩ directions (Λ) or at L points in the Brillouin zone. These critical points are of the M_1 type. The longitudinal effective mass, however, is much larger than its transverse counterparts and one can treat these CP's as two-dimensional (2D) minima. The contribution to $\epsilon_1(\omega)$ and $\epsilon_2(\omega)$ of this type of 2D minima is given by[5]

$$\epsilon_1(\omega) - 1 = -B_1\chi_1^{-2}\ln(1-\chi_1^2) - B_2\chi_{1s}^{-2}\ln(1-\chi_{1s}^2), \tag{8}$$

$$\epsilon_2(\omega) = \pi[B_1\chi_1^{-2}H(\chi_1 - 1) + B_2\chi_{1s}^{-2}H(\chi_{1s} - 1)], \tag{9}$$

with

$$\chi_1 = \hbar\omega/E_1, \tag{10a}$$

$$\chi_{1s} = \hbar\omega/(E_1 + \Delta_1), \tag{10b}$$

where B's are the strength parameters and H's are functions defined by Eq. (7).

The more pronounced structure found in the higher energy region than $E_1/(E_1 + \Delta_1)$ is usually labeled E_2. The nature of the E_2 transitions is more complicated, since it does not correspond to a single, well-defined CP. Because of this fact, we shall characterize the E_2 structure as that of a damped harmonic oscillator[5]:

$$\epsilon_1(\omega) - 1 = C(1-\chi_2^2)/[(1-\chi_2^2)^2 + \chi_2^2\gamma^2]. \tag{11}$$

$$\epsilon_2(\omega) = C\chi_2\gamma/[(1-\chi_2^2)^2 + \chi_2^2\gamma^2], \tag{12}$$

with

$$\chi_2 = \hbar\omega/E_2, \tag{13}$$

where C is the strength parameter and γ is the damping factor.

Combining all these contributions, one can obtain the spectral dependence of ϵ_1 and ϵ_2 in the entire range of photon energies. Figures 1 and 2 show, as examples, the ϵ_1 and ϵ_2 spectra of InSb in the energy range 0–7.0 eV. The solid line in Fig. 1 is taken by the sum of Eqs. (2), (8), and (11), and the solid line in Fig. 2 is taken by the sum of Eqs. (3), (9), and (12). The numerical values used are as follows: $E_0 = 0.18$ eV; $\Delta_0 = 0.81$ eV; $E_1 = 1.80$ eV; $E_2 = 3.9$ eV; $A = 0.19$; $B_1 = 6.37$; $C = 5.37$; and $\gamma = 0.318$. Since the E_1 transitions can contain sufficient strength to represent both E_1 and $E_1 + \Delta_1$, the contribution of the latter gap is neglected here. Equation (8) shows a singularity at $\hbar\omega = E_1$. To overcome

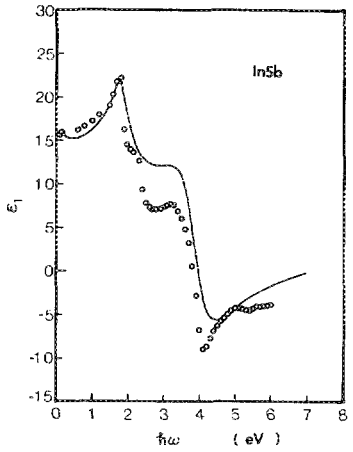

FIG. 1. ϵ_1 spectrum of InSb. The experimental data (open circles) are taken from Ref. b of Table III and from D. E. Aspnes and A. A. Studna, Phys. Rev. B **27**, 985 (1983). The solid line is obtained from the sum of Eqs. (2), (8), (11), and $\epsilon_{1\infty}$ (= 3.1).

this problem, we introduced the damping effect in Eq. (8) in a phenomenological manner by replacing ω by $\omega + i(\Gamma_s/\hbar)$ ($\Gamma_s = 0.16$ eV). Moreover, we considered an additional constant-background contribution $\epsilon_{1\infty}$ (= 3.1) to ϵ_1 in order to account for other higher-lying CP transitions (E_0', $E_0' + \Delta_0'$, E_1', $E_1' + \Delta_1'$, etc.).

We show in Fig. 3 an individual contribution to ϵ_1 of the $E_0/E_0 + \Delta_0$, E_1, and E_2 gaps for InSb. The $E_0/E_0 + \Delta_0$-gap contribution becomes appreciable only in the photon-energy region close to these gaps. The E_1- and E_2-gap contributions are found to be nearly constant in the region near the $E_0/E_0 + \Delta_0$ gap.

Since our analysis will be made below the E_0 gap, it is sufficient to consider only the $E_0/E_0 + \Delta_0$ gap as the dispersion mechanism. Thus, we can obtain

$$\epsilon_1(\omega) = A\,[f(\chi_0) + \tfrac{1}{2}[E_0/(E_0+\Delta_0)]^{1.5} f(\chi_{os})] + B, \tag{14}$$

where B is the constant term arising mainly from the E_1 and E_2 gaps. Since $\epsilon_2(\omega)$ may be taken as zero in the region near and below the E_0 gap, one can also obtain

$$n(\omega) \simeq \epsilon_1(\omega)^{0.5}. \tag{15}$$

B. Material parameters of quaternary alloys

There has been considerable interest in the quaternary III-V compounds for many device applications. However,

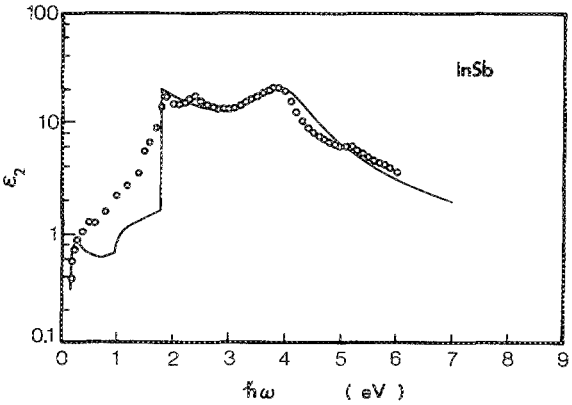

FIG. 2. ϵ_2 spectrum of InSb. The experimental data (open circles) are taken from Ref. b of Table III and from D. E. Aspnes and A. A. Studna, Phys. Rev. B **27**, 985 (1983). The solid line is obtained from the sum of Eqs. (3), (9), and (12).

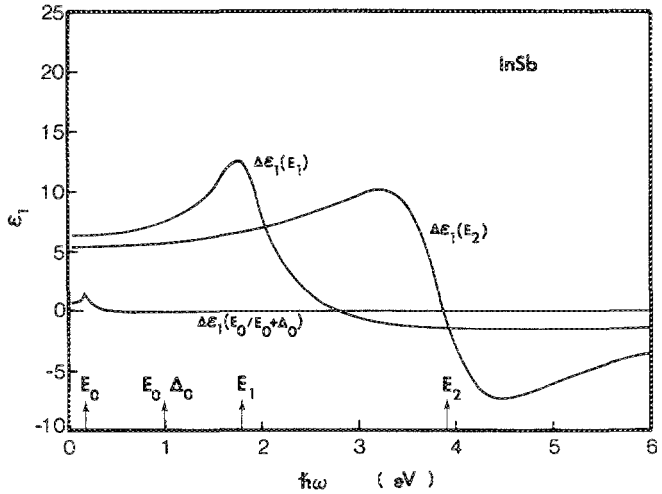

FIG. 3. Individual contribution to ϵ_1 of the $E_0/E_0+\Delta_0$, E_1, and E_2 gaps for InSb.

some practical device parameters in these materials have been hampered by a lack of definite knowledge of many material parameters. An interpolation scheme is known to be a useful tool for estimating some material parameters of alloy compounds.[2] Although the scheme is still open to experimental verification, it provides more reliable values over the entire range of alloy composition.

Quaternary alloy is thought to be constructed of four or three binary compounds: AC, AD, BC, and BD with compositions of the form $A_x B_{1-x} C_y D_{1-y}$ or AB, AC, and AD with compositions of the form $AB_x C_y D_{1-x-y}$. The quaternary material parameter Q can thus be estimated from these binary parameters (B's) by using the interpolation scheme:

$$Q(x,y) = xyB_{AC} + x(1-y)B_{AD} + (1-x)yB_{BC} + (1-x)(1-y)B_{BD} \quad (16a)$$

or

$$Q(x,y) = xB_{AB} + yB_{AC} + (1-x-y)B_{AD}. \quad (16b)$$

If relationships for the ternary material parameters (T's) are available [see Eq. (19)], the quaternary parameter can be expressed either as $(A_x B_{1-x} C_y D_{1-y})$ (Ref. 2)

$$Q(x,y) = \frac{x(1-x)[yT_{ABC}(x) + (1-y)T_{ABD}(x)] + y(1-y)[xT_{ACD}(y) + (1-x)T_{BCD}(y)]}{x(1-x) + y(1-y)} \quad (17a)$$

or $(AB_x C_y D_{1-x-y})$ (Ref. 6),

$$Q(x,y) = \frac{xyT_{ABC}(u) + y(1-x-y)T_{ACD}(v) + (1-x-y)xT_{ABD}(w)}{xy + y(1-x-y) + (1-x-y)x} \quad (17b)$$

with

$$u = (1-x-y)/2, \quad (18a)$$

$$v = (2-x-2y)/2, \quad (18b)$$

and

$$w = (2-2x-y)/2. \quad (18c)$$

The lattice constant "a" is known to obey Vegard's law well, i.e., to vary linearly with composition [Eq. (16)]. In Sec. III, we shall obtain the lattice matching conditions for quaternary alloys on GaSb or InAs substrate by using this Vegard's law. The band gaps in many ternary alloys can be approximated in the form of a quadratic function:

$$T_{ABC}(x) = xT_{AC} + (1-x)T_{BC} + Cx(x-1), \quad (19)$$

where C is referred to as a bowing parameter. In Table I, we present the lattice constants and the band-gap energies for the III-V binary compounds of interest. Table II also lists the bowing parameters of various band gaps for the III-V ternary alloys. Relatively few of the bowing parameters are known with any uncertainty, especially for the $\Gamma - X(C_X)$ and the $\Gamma - L$ indirect band gaps (C_L). Some of the unknown bowing parameters are estimated in this study from the following assumptions:

$$C_X \simeq 1/2(C_0 + C_2), \quad (20a)$$

$$C_L \simeq 1/2(C_0 + C_1), \quad (20b)$$

where C_0, C_1, and C_2 are the bowing parameters of the E_0, E_1, and E_2 gaps, respectively. To estimate the bowing parameters of the Δ_0 gap, we used Hill's model,[7] which attributes to the nonlinearity of E_0 and Δ_0 the same physical origin:

$$C_\Delta \simeq (\Delta_{01}/E_{01})C_0, \quad (21)$$

where Δ_{01} and E_{01} are the linearly interpolated values of Δ_0 and E_0 ($x = 0.5$) from the limiting compounds. The quaternary band gaps as a function of composition are obtained by numerical solution of Eq. (17), using the data given in Tables I and II. These values are also used to calculate the dispersion of the refractive indices of the quaternary alloys.

TABLE I. Lattice constants and band-gap energies of III-V binary compounds (RT).

Binary	Lattice constant a (Å)	Band-gap energy (eV)			
		E_0	Δ_0	E_g^X	E_g^L
AlAs	5.6611	2.95	0.28	2.16	2.36
AlSb	6.1355	2.30	0.72	1.61	2.21
GaAs	5.6533	1.42	0.34	1.91	1.73
GaSb	6.0959	0.72	0.74	1.05	0.76
InP	5.8688	1.35	0.10	2.21	2.05
InAs	6.0584	0.36	0.40	1.37	1.07
InSb	6.4794	0.18	0.81	1.63	0.93

III. ANALYSIS AND DISCUSSION

The mechanisms, which we omitted from this analysis but which may affect the index of refraction near or below

TABLE II. Bowing parameters of III-V ternary compounds (RT).

Ternary	Bowing parameter (eV)			
	C_0	C_Δ	C_X	C_L
(Al,Ga)As	0.37[a]	0.07[b]	0.245[a]	0.055[a]
(Ga,In)As	0.6[c]	0.20[b]	1.4[d]	0.72[d]
(Al,Ga)Sb	0.47[e]	0.3[e]	0[e]	0.55[e]
(Ga,In)Sb	0.42[f]	0.1[f]	0.33[g]	0.38[g]
Al(As,Sb)	0	0	0	0
Ga(As,Sb)	1.2[h]	0.61[i]	1.09[g]	1.09[g]
In(P,As)	0.28[j]	0.16[b]	0.28[g]	0.27[g]
In(P,Sb)	1.6[k]	0.95[i]	1.56[g]	1.6[g]
In(As,Sb)	0.58[l]	1.2[b]	0.59[g]	0.57[g]

[a] H. J. Lee *et al.*, Phys. Rev. B **21**, 659 (1980).
[b] O. Berolo *et al.*, Phys. Rev. B **8**, 3794 (1973).
[c] K.-R. Schulze *et al.*, Phys. Status Solidi B **75**, 493 (1976).
[d] W. Porod and D. K. Ferry, Phys. Rev. B **27**, 2587 (1983).
[e] C. Alibert *et al.*, Phys. Rev. B **27**, 4946 (1983).
[f] D. Auvergne *et al.*, J. Phys. Chem. Solids **35**, 133 (1974).
[g] Estimated in this study (see text).
[h] M. B. Thomas *et al.*, Phys. Status Solidi A **37**, K173 (1976).
[i] Calculated as described in the text.
[j] I. V. Bodnar *et al.*, Phys. Status Solidi A **37**, K173 (1976).
[k] T. Fukui and Y. Horikoshi, Jpn. J. Appl. Phys. **20**, 587 (1981).
[l] S. S. Vishnubhatla *et al.*, Can. J. Phys. **47**, 1661 (1969).

the E_0 gap, are the indirect-gap transitions, the free-carrier absorptions, the lattice vibrational effect, and the crystalline-imperfection effect. When the absorption at the optical energy gap is indirect, as in GaP, the associated dispersion in the index would be much less pronounced than for the cases we have considered in Sec. II, and a peak in the refractive-index dispersion is unlikely to occur near such an edge. The free-carrier associated dispersion in the index can be expressed in the form $n^2 = -Ne^2/m\epsilon_0\omega^2$, where N is the concentration of free carriers and m is their susceptibility mass. This effect can be important only at wavelengths smaller than 10 μm. The dispersion associated with lattice vibrations can become important only when $\hbar\omega \simeq \hbar\omega_{TO}$ (where $\hbar\omega_{TO}$ is the energy of the transverse optical lattice vibration modes of long wavelength) and is negligible in this region of interest. One should also note that some crystalline-imperfection effect may strongly affect the index of refraction, especially in the region very close to the E_0 gap. Knowledge of the refractive-index dispersion in the E_0-gap region forms a very important part in the design of semiconductor lasers. Because no reliable data are available in this energy region, we are forced to neglect this effect in our calculation. However, one can obtain detailed information on this effect in the Appendix.

A. $Al_xGa_{1-x}As_ySb_{1-y}$

Lattice matching condition:
(GaSb sub.)

$$y = \frac{0.0396x}{0.4426 + 0.0318x} \quad (0 \leqslant x \leqslant 1.0), \tag{22a}$$

(InAs sub.)

$$y = \frac{0.0375 + 0.0396x}{0.4426 + 0.0318x} \quad (0 \leqslant x \leqslant 1.0). \tag{22b}$$

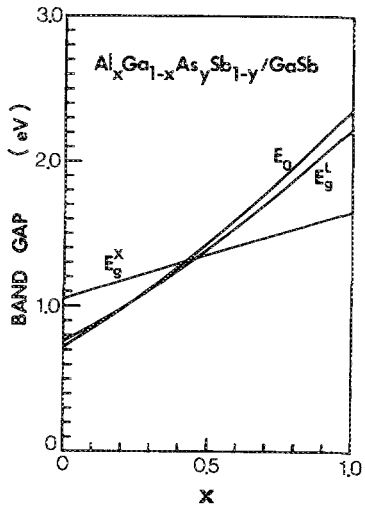

FIG. 4. Band-gap energies as a function of the x-composition parameter for $Al_xGa_{1-x}As_ySb_{1-y}$ lattice matched to GaSb.

The $Al_xGa_{1-x}As_ySb_{1-y}$ quaternary alloys are important materials covering the wavelengths between the visible and infrared region (0.57–1.72 μm) suitable for device applications, such as injection lasers,[8–11] photodiodes,[12,13] and solar cells.[14] These alloys are also interesting materials for cladding layers of the GaInAsSb/AlGaAsSb injection lasers (see Sec. III B). The alloys can be grown lattice matched to commercially available binary substrates GaSb, InP, and InAs. The existence of extensive miscibility gaps in these lattice matching systems may, however, limit the range of homogeneous solid-phase compositions. This is especially the case for the AlGaAsSb/InP and AlGaAsSb/InAs systems. Nevertheless, Chiu *et al.*[15] have recently demonstrated the possiblity of growing quaternary alloys (AlGaAsSb/InP) having compositions within the miscibility gap using nonequilibrium growth method (molecular beam epitaxy).

Figures 4 and 5 show, respectively, the band-gap energies (E_0,E_g^X, and E_g^L) as a function of the x-composition parameter for $Al_xGa_{1-x}As_ySb_{1-y}$ lattice matched to GaSb and InAs. One can see from these figures that the systems show a transition between the direct and indirect structures at compositions of about $x \simeq 0.45$. It is worth noting, moreover, that the E_0 value in the direct-gap region of these sys-

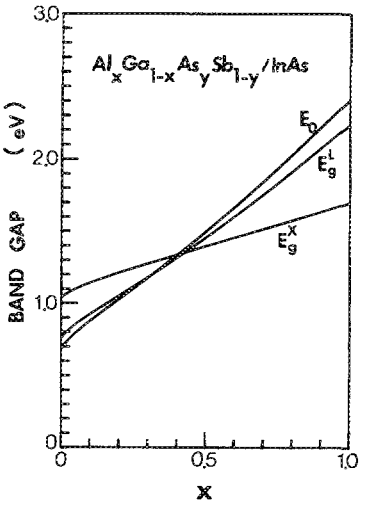

FIG. 5. Band-gap energies as a function of the x-composition parameter for $Al_xGa_{1-x}As_ySb_{1-y}$ lattice matched to InAs.

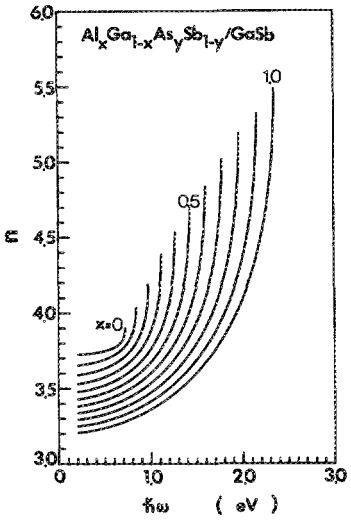

FIG. 6. Calculated refractive indices of $Al_xGa_{1-x}As_ySb_{1-y}$/GaSb as a function of the photon energy with x-composition increments of 0.1.

tems is very close to the lowest indirect-gap energy (E_g^L). This degeneracy of the conduction band at the Γ and L points is known to result in a large threshold current, owing to an injected-electron loss in the L valleys. Relatively large values of Δ_0 in these systems should also cause the nonradiative Auger recombination and intervalence-band optical transitions involving the Δ_0 gap to deteriorate the laser-operation characteristics (threshold current and its temperature dependence). One can find a detailed discussion of this problem in Refs. 16 and 17.

The calculated refractive indices of these systems as a function of the photon energy with x-composition increments of 0.1 are shown in Figs. 6 and 7. The curves higher-energy endpoints correspond to the values of n at the lowest direct gaps E_0. Table III shows the values of A and B required to fit the experimental III-V binary data to Eq. (14). Our previous studies[2,3] showed that the values of A and B varied almost linearly with composition for such alloy semiconductors as $Al_xGa_{1-x}As$ and $In_{1-x}Ga_xAs_yP_{1-y}$. Based on this fact, the quaternary values of A and B are obtained from numerical solutions of Eq. (16), using the data listed in Table III.

The important bearing of the refractive index on the operation of an injection laser is its role in the confinement of

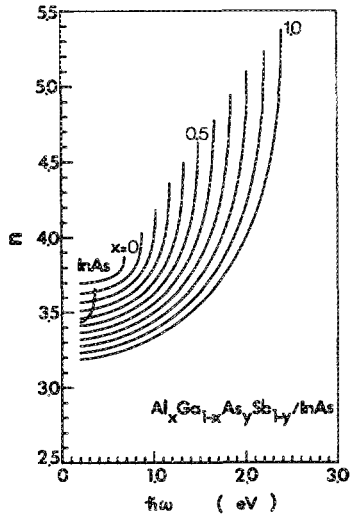

FIG. 7. Calculated refractive indices of $Al_xGa_{1-x}As_ySb_{1-y}$/InAs as a function of the photon energy with x-composition increments of 0.1.

TABLE III. Parameters A and B used in the calculation of $\epsilon_1(\omega)$.

Binary	A	B
AlAs[a]	25.30	−0.80
AlSb[b]	59.68	−9.53
GaAs[c]	6.3	9.4
GaSb[b]	4.05	12.66
InP[d]	8.40	6.60
InAs[b]	5.14	10.15
InSb[b]	7.91	13.07

[a] R. E. Fern and A. Onton, J. Appl. Phys. **42**, 3499 (1971).
[b] B. O. Seraphin and H. E. Bennett, *Semiconductors and Semimetals*, edited by R. K. Willardsson and A. C. Beer (Academic, New York, 1967), Vol. 3, p. 499.
[c] H. C. Casey, Jr. *et al.*, Appl. Phys. Lett. **24**, 63 (1974).
[d] G. D. Pettit and W. J. Turner, J. Appl. Phys. **36**, 2081 (1965).

the emitted radiation to the intermediate vicinity of an active region.[4] As can be seen from Figs. 6 and 7, the AlGaAsSb/GaSb and AlGaAsSb/InAs systems provide a large refractive index step within a whole range of the x composition for the light confinement in an active region. The refractive index and its dependence on x and photon energy also show a case that is usual for $Al_xGa_{1-x}As$/GaAs and $In_{1-x}Ga_xAs_yP_{1-y}$/InP systems.[2,3]

B. $Ga_xIn_{1-x}As_ySb_{1-y}$

Lattice matching condition:
(GaSb sub.)

$$y=\frac{0.3835-0.3835x}{0.4210+0.216x} \quad (0\leqslant x\leqslant 1.0), \tag{23a}$$

(InAs sub.)

$$y=\frac{0.4210-0.3835x}{0.4210+0.0216x} \quad (0\leqslant x\leqslant 1.0). \tag{23b}$$

Advances in optoelectronic devices usually rely on progress achieved in the optical fiber fields. The 2–4-μm spectral region is currently of great interest because of the recent development of low-loss fluoride glass fibers in this spectral region.[1] The predicted loss of these fibers is two or three orders of magnitude lower than those of conventional silica fibers. The $Ga_xIn_{1-x}As_ySb_{1-y}$ quaternary system offers interesting possibilities, because they can provide the basis for devices operating over this entire spectral region.

The alloy system $Ga_xIn_{1-x}As_ySb_{1-y}$ has received relatively little attention until recently because it has a very large miscibility gap with a relatively high critical temperature ($\sim$1470 °C).[18,19] Nevertheless, several papers have already reported injection lasers based on this alloy system. Kobayashi, Horikoshi, and Uemura[20] have demonstrated pulsed room-temperature (RT) operation of GaInAsSb/AlGaAsSb lasers emitting at 1.8 μm with threshold current densities (J_{th}) of 5 kA/cm^2. At longer wavelengths,[21] pulsed GaInAsSb/AlGaAsSb injection lasers have operated at RT with J_{th} = 13 and 20 kA/cm^2 at 2 and 2.3 μm, respectively. Caneau *et al.*[22] have also achieved RT pulsed operation of GaInAsSb/AlGaAsSb lasers emitting at 2.2 μm with J_{th} = 7 kA/cm^2. They have also demonstrated continuous operation of GaInAsSb/AlGaAsSb lasers at 2.1 μm up to a temperature of 190 K and, more recently, up to near

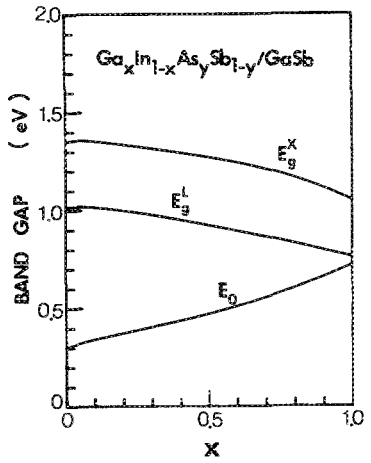

FIG. 8. Band-gap energies as a function of the x-composition parameter for $Ga_xIn_{1-x}As_ySb_{1-y}$ lattice matched to GaSb.

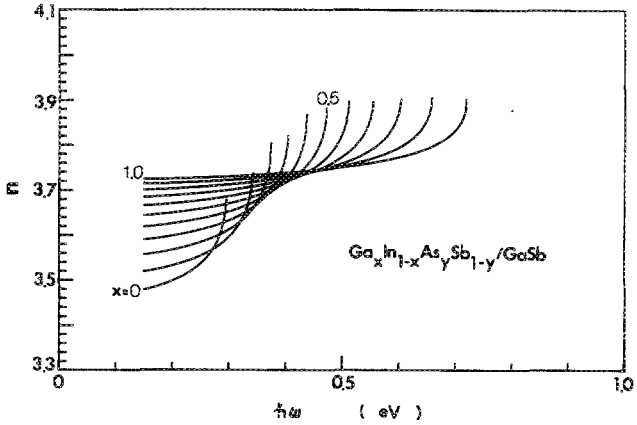

FIG. 10. Calculated refractive indices of $Ga_xIn_{1-x}As_ySb_{1-y}/GaSb$ as a function of the photon energy with x-composition increments of 0.1.

RT.[23] However, to our knowledge, there have been no detailed reports on the refractive index and its variation with material composition and wavelength for $Ga_xIn_{1-x}As_ySb_{1-y}$ quaternary alloys. Reliable band-gap data are also lacking as yet for these alloys over the entire range of composition.

The band-gap energies as a function of the x-composition parameter for $Ga_xIn_{1-x}As_ySb_{1-y}$ lattice matched to GaSb and InAs are shown in Figs. 8 and 9, repectively. Like $Al_xGa_{1-x}As_ySb_{1-y}$, the $Ga_xIn_{1-x}As_ySb_{1-y}$, quaternaries may be grown lattice matched to GaSb, InP, and InAs. Lattice matched to InP, the band-gap energy is nearly fixed, ranging from 0.71–0.86 eV. Lattice matched to GaSb and InAs, on the other hand, the energy varies in the range 0.30–0.71 eV (4.1–1.7 μm) and 0.36–0.69 eV (3.4–1.8 μm), respectively. Unlike $Al_xGa_{1-x}As_ySb_{1-y}$, moreover, the absorption at the fundamental optical gaps in the $Ga_xIn_{1-x}As_ySb_{1-y}$/GaSb and $Ga_xIn_{1-x}As_ySb_{1-y}$/InAs quaternaries is expected to be direct within a whole range of the x composition ($0 \leqslant x \leqslant 1.0$). It is also clear from the figures that the conduction-band minimum at the Γ point is much lower than those at the L and X points, especially for smaller values of x.

Figures 10 and 11 show, respectively, the calculated refractive indices of $Ga_xIn_{1-x}As_ySb_{1-y}$ lattice matched to GaSb and InAs with x-composition increments of 0.1. A noticeable feature found in these figures is that the systems show a refractive-index anomaly, i.e., the smaller E_0-gap material has a smaller value of the refractive index. Most of the III-V compound alloys, like $Al_xGa_{1-x}As$, $In_{1-x}Ga_xAs_yP_{1-y}$, and $Al_xGa_{1-x}As_ySb_{1-y}$, show that the smaller E_0-gap material has a larger value of the refractive index.

If the refractive index in the active region of an injection laser is smaller than the index of the cladding layer on both sides, the effect is like that of an antiwaveguide configuration which does not confine radiation to the neighborhood of the active region. This effect offers an optical loss in the waveguide, leading to an increase of the threshold current. Since the refractive indices of $Al_xGa_{1-x}As_ySb_{1-y}$ alloys are usually greater than those of $Ga_xIn_{1-x}As_ySb_{1-y}$ alloys, $Al_xGa_{1-x}As_ySb_{1-y}$ cladding layers make a strong combination with a $Ga_xIn_{1-x}As_ySb_{1-y}$ active layer to confine sufficiently the radiation from such an injection laser.[20]

The origin of the refractive-index anomaly is of particular interest. A series of our calculations also suggested such an anomaly in the Sb-based compound alloys (e.g., $InAs_xSb_{1-x}$, $Al_xIn_{1-x}P_ySb_{1-y}$, and $GaP_xAs_ySb_{1-x-y}$). If we try to generalize the refractive-index behaviors of III-V binary compounds, we can classify them into two groups, i.e., the As(P)-based and the Sb-based compounds. Each group shows no refractive-index anomaly, but the Sb-based compounds give considerably

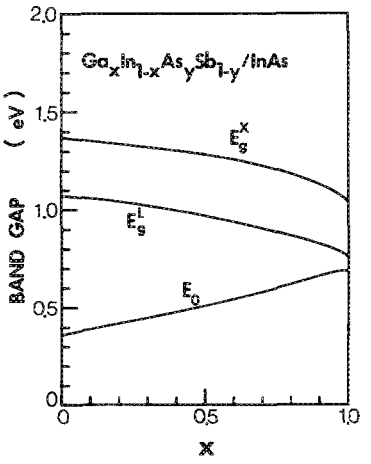

FIG. 9. Band-gap energies as a function of the x-composition parameter for $Ga_xIn_{1-x}As_ySb_{1-y}$ lattice matched to InAs.

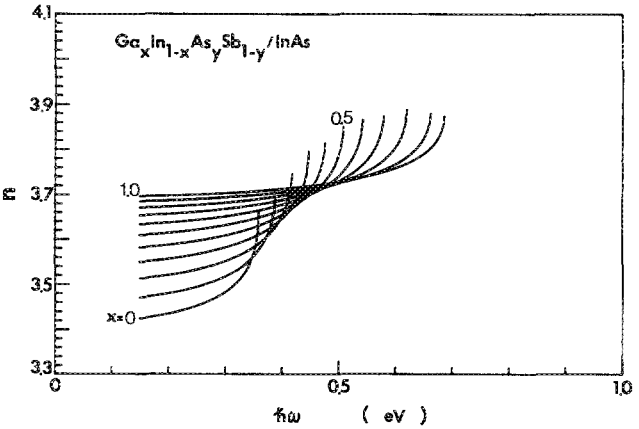

FIG. 11. Calculated refractive indices of $Ga_xIn_{1-x}As_ySb_{1-y}$/InAs as a function of the photon energy with x-composition increments of 0.1.

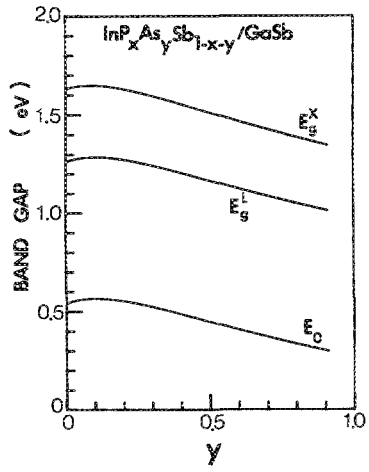

FIG. 12. Band-gap energies as a function of the y-composition parameter for $InP_xAs_ySb_{1-x-y}$ lattice matched to GaSb.

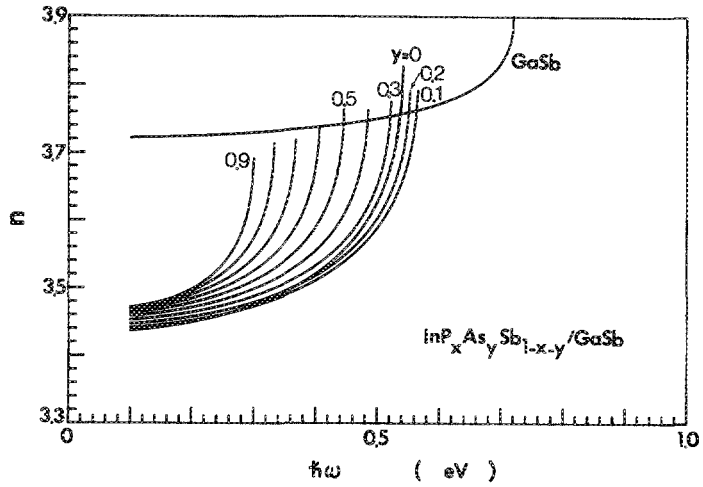

FIG. 14. Calculated refractive indices of $InP_xAs_ySb_{1-x-y}$/GaSb as a function of the photon energy with y-composition increments of 0.1.

larger refractive indices than the As(P)-based one and, as a result, they don't fuse each other. Moreover, as mentioned in Sec. II, the refractive indices of solids are strongly connected with their electronic energy-band structures. It is known[24] that the band-structure related constants, such as the band-gap energies and band masses, in the Sb-based ternaries exhibit strong nonlinearity with respect to the alloy composition which arises from the effects of alloy disorder. The refractive-index anomaly found in the Sb-based III-V alloys seems to be a consequence of these facts.

C. $InP_xAs_ySb_{1-x-y}$

Lattice matching condition:
(GaSb sub.)

$$x = 0.6281 - 0.6895y \quad (0 \leqslant y \lesssim 0.91), \tag{24a}$$

(InAs sub.)

$$x = 0.6895 - 0.6895y \quad (0 \leqslant y \leqslant 1.0). \tag{24b}$$

Like $Ga_xIn_{1-x}As_ySb_{1-y}$, the alloys $InP_xAs_ySb_{1-x-y}$ have promising applications as light sources and detectors for long-wavelength communication system. The growth of the $InP_xAs_ySb_{1-x-y}$ quaternaries has been previously reported,[25,26] and lasers using electron injection,[27] electron beam pumping,[28] and optical pumping[29] have been described. Infrared emission up to 4.6 μm has also been reported from single-heterostructure $InP_xAs_ySb_{1-x-y}$ diodes.[30]

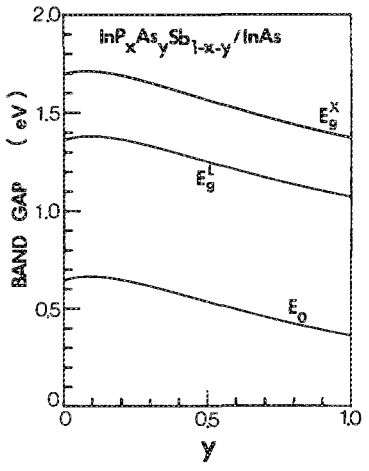

FIG. 13. Band-gap energies as a function of the y-composition parameter for $InP_xAs_ySb_{1-x-y}$ lattice matched to InAs.

The band-gap energies as a function of the y-composition parameter for $InP_xAs_ySb_{1-x-y}$ lattice matched to GaSb and InAs are shown in Figs. 12 and 13, respectively. These quaternaries have direct gaps as the fundamental absorption edges within a full range of the y composition. The direct-gap energies between 0.30 and 0.57 eV can be obtained for the quaternaries lattice matched to GaSb and between 0.36–0.66 eV for the quaternaries lattice matched to InAs. These values are much lower than the lowest indirect gap energies (E_g^L).

The calculated refractive indices of these systems as a function of the photon energy with y-composition increments of 0.1 are shown in Figs. 14 and 15. The refractive-index anomaly occurs only in the region of smaller y compositions ($y \lesssim 0.2$). The long-wavelength indices do not differ as much with the y composition. It is evident from these figures that $InP_xAs_ySb_{1-x-y}$ lasers require an active layer of larger y and cladding layers of smaller y compositions in order to obtain sufficient optical confinement.

IV. CONCLUSION

AlGaAsSb, GaInAsSb, and InPAsSb quaternary systems have attracted great interest because of the recent de-

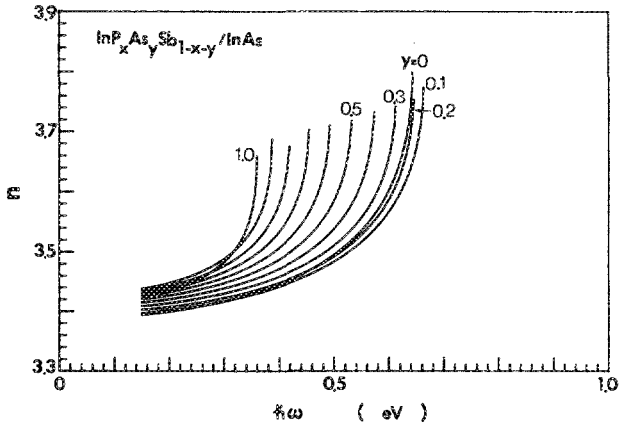

FIG. 15. Calculated refractive indices of $InP_xAs_ySb_{1-x-y}$/InAs as a function of the photon energy with y-composition increments of 0.1.

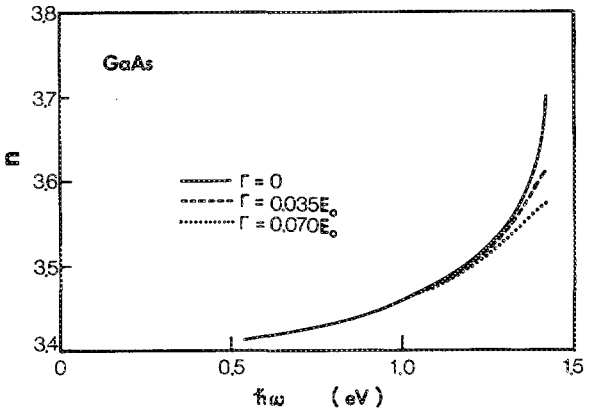

FIG. 16. Calculated refractive-index dispersion of GaAs with three different damping parameters ($\Gamma = 0$, 0.035 E_0, and 0.070 E_0).

velopment of low-loss optical fibers in the 2–4-μm wavelength region. A number of interesting semiconductor properties of the quaternary systems require quite detailed knowledge of material parameters for their analysis, but it is, at present, rather difficult to obtain the most reliable values from the literature reported. The models for calculation of various device parameters (the lattice constant, the band-gap energy, and the refractive index) in compound alloys are discussed, and the results for AlGaAsSb, GaInAsSb, and InPAsSb quaternaries lattice matched to GaSb and InAs are presented. Key properties of the quaternary material parameters for a variety of optoelectronic-device applications are also discussed in detail.

ACKNOWLEDGMENT

The author would like to thank Dr. T. Ikegami for pointing out an anomaly of the refractive index in the Sb-based alloys, and for advice during the course of this work.

APPENDIX

The impurities or, more generally, the lattice defects in semiconductors, reduce the lifetime of the electronic states (excitons and/or free electron-hole pairs) resulting in a change in the optical properties. The refractive-index dispersion may be affected by the lifetime broadening of the electronic states, especially in the photon-energy region close to the band edge. We can easily introduce such an effect in our model in a phenomenological manner by replacing $\hbar\omega$ in Eq. (2) by $\hbar\omega + i\Gamma$, where Γ is the broadening energy. Figure 16 shows, as an example, calculated refractive-index dispersion of GaAs with three different damping parameters; $\Gamma = 0$, $\Gamma = 0.035\ E_0$, and $\Gamma = 0.070\ E_0$. It is obvious from this figure that the broadening effect considerably reduces the n value, especially in the E_0-gap region. One must, therefore, pay attention to the analysis of the refractive-index dispersion in such a region.

[1]R. W. France, S. F. Carter, J. R. Williams, K. J. Beales, and J. M. Parker, Electron. Lett. **20**, 607 (1984).
[2]S. Adachi, J. Appl. Phys. **53**, 8775 (1982); **54**, 1844 (1983); **54**, 6620 (1983); **56**, 74 (1984); **56**, 1499 (1984); **58**, R1(1985).
[3]S. Adachi, J. Appl. Phys. **53**, 5863 (1982).
[4]H. C. Casey, Jr. and M. B. Panish, *Heterostructure Lasers* (Academic, New York, 1978), Parts A and B.
[5]S. Adachi, Phys. Rev. B (in press).
[6]C. K. Williams, T. H. Glisson, J. R. Hauser, and M. A. Littlejohn, J. Electron. Mater. 7, 639 (1978).
[7]R. Hill, J. Phys. C 7, 516 (1974).
[8]R. E. Nahory, M. A. Pollack, E. D. Beebe, J. C. DeWinter, and R. W. Dixon, Appl. Phys. Lett. **28**, 19 (1976).
[9]A. Sasaki, M. Nishimura, and Y. Takeda, Jpn. J. Appl. Phys. **19**, 1695 (1980).
[10]Y. A. Aarik, L. M. Dolginov, A. E. Drakin, L. V. Druzhinina, P. G. Eliseev, P. A. Lyuk, B. N. Sverdlov, V. A. Skripkin, and Y. F. Friedentkhal, Sov. J. Quantum Electron. **10**, 50 (1980).
[11]L. M. Dolginov, A. E. Drakin, L. V. Druzhinina, P. G. Eliseev, M. G. Milvidsky, V. A. Skripkin, and B. N. Sverdlov, IEEE J. Quantum Electron. **QE-17**, 593 (1981).
[12]T. P. Pearsall, R. E. Nahory, and M. A. Pollack, Appl. Phys. Lett. **28**, 403 (1976).
[13]T. Kagawa and G. Motosugi, Jpn. J. Appl. Phys. **20**, 597 (1981).
[14]M. L. Timmons, S. M. Bedair, R. J. Markunas, and J. A. Hutchby, *Conference Record of the 16th IEEE Photovoltaic Specialists Conference* (IEEE, New York, 1982), p. 663.
[15]T. H. Chiu, W. T. Tsang, S. N. G. Chu, J. Shah, and J. A. Ditzenberger, Appl. Phys. Lett. **46**, 408 (1985).
[16]M. G. Burt, J. Phys. C **14**, 3269 (1981).
[17]M. Takeshima, J. Appl. Phys. **56**, 2502 (1984).
[18]J. C. DeWinter, M. A. Pollack, A. K. Srivastava, and J. L. Zyskind, J. Electron. Mater. **14**, 729 (1985).
[19]M. Astles, H. Hill, A. J. Williams, P. J. Wright, and M. L. Young, J. Electron. Mater. **15**, 41 (1986).
[20]N. Kobayashi, Y. Horikoshi, and C. Uemura, Jpn. J. Appl. Phys. **19**, L 30 (1980).
[21]A. E. Bochkarev, L. M. Dolginov, A. E. Drakin, L. V. Druzhinina, P. G. Eliseev, and B. N. Sverdlov, Sov. J. Quantum Electron. **15**, 869 (1985).
[22]C. Caneau, A. K. Srivastava, A. G. Dentai, J. L. Zyskind, and M. A. Pollack, Electron. Lett. **21**, 815 (1985).
[23]C. Caneau, A. K. Srivastava, J. L. Zyskind, J. W. Sulhoff, A. G. Dentai, and M. A. Pollack, Appl. Phys. Lett. **49**, 55 (1986).
[24]See, for example, O. Berolo, J. C. Woolley, and J. A. van Vechten, Phys. Rev. B **8**, 3794 (1973).
[25]T. Fukui and Y. Horikoshi, Jpn. J. Appl. Phys. **20**, 587 (1981).
[26]N. Kobayashi and Y. Horikoshi, Jpn. J. Appl. Phys. **20**, 2301 (1981).
[27]N. Kobayashi and Y. Horikoshi, Jpn. J. Appl. Phys. **19**, L 641 (1980).
[28]L. M. Dolginov, Y. N. Korchagin, I. V. Kryukova, V. I. Leskovich, E. V. Matveenko, M. G. Mil'vidskii, and V. M. Stepanov, Sov. Tech. Phys. Lett. **4**, 580 (1978).
[29]J. P. van der Ziel, R. A. Logan, R. M. Mikulyak, and A. A. Ballman, IEEE J. Quantum Electron. **QE-21**, 1827 (1985).
[30]N. P. Esina, N. V. Zotova, B. A. Matveev, N. M. Stus', G. N. Talalakin, and T. D. Abishev, Sov. Tech. Phys. Lett. **9**, 167 (1983).